JAAS

ROYAL SOCIETY OF CHEMISTRY

PAPER

View Article Online
View Journal | View Issue

Cite this: *J. Anal. At. Spectrom.*, 2023, **38**, 1865

Reference-free X-ray fluorescence analysis using well-known polychromatic synchrotron radiation†

André Wählisch, * Malte Wansleben, ‡ Rainer Unterumsberger, ‡ Yves Kayser § and Burkhard Beckhoff

Received 5th April 2023
Accepted 3rd July 2023

DOI: 10.1039/d3ja00109a

rsc.li/jaas

A reliable X-ray fluorescence (XRF) analysis can be achieved by using accurate knowledge of the spectral distribution of the excitation source. Since most commonly employed X-ray sources emit broadband polychromatic radiation, it is essential to fully characterize the source in order to calculate its spectrum under varying operational settings. By using the calculable synchrotron radiation from a bending magnet, this work shows that a reference-free XRF approach can be implemented for polychromatic excitation conditions. It is further demonstrated that this physically traceable approach is capable of quantifying thin layers as well as stratified materials. The same principles may readily be transferred to similar polychromatic X-ray sources, such as XRF instruments based on an X-ray tube.

1 Introduction

X-ray fluorescence (XRF) analysis is a versatile analytical technique used mainly to determine the elemental composition of bulk samples (e.g., alloys, geological material, cultural heritage specimens)[1–4] and can also be employed to determine the (mass) thickness of μm down to sub-nm layers (e.g., semiconductors, coatings, corrosion layers).[5–8] The photoionization process—which results in the emission of the characteristic XRF radiation—can be induced by a wide range of different excitation sources. Common photon-based X-ray sources include, for example, radiation from conventional X-ray tubes and synchrotron radiation (SR). Since these X-ray sources themselves are based on different physical principles, they reveal significant dissimilarities with regard to various characteristics, such as intensity, beam size, beam divergence, spectral distribution, polarization, and availability. Therefore, their suitability for a specific XRF application can vary considerably. The unpolarized radiation from conventional X-ray tubes is mainly composed of a polychromatic bremsstrahlung component and several monochromatic characteristic lines. As such, different chemical elements may be excited and studied simultaneously by XRF based on this polychromatic excitation. Most notably, if a multitude of chemical elements are of interest, information about all of them may be gained in a single "shot". In contrast, the linearly polarized radiation from a bending magnet at SR facilities has a solely polychromatic spectral distribution from which a specific monochromatic part is usually selected by means of a monochromator. The resulting tunability can be used to selectively probe individual chemical elements sequentially. This means that for SR the excitation conditions can be tailored to probe a few chemical elements at a time, while ensuring optimal sensitivity and quantification reliability. Consequently, the differences in spectral characteristics are reflected in the varying quantification capabilities of these distinct X-ray sources.[9–12]

Nevertheless, both types of excitation sources, X-ray tube and SR, induce the emission of the characteristic XRF radiation in the same way. In fact, the number of induced XRF photons resulting from excitation by an X-ray tube and by SR may be described by the same relationship incorporating experimental, instrumental, and atomic fundamental parameters (FPs). Quantitative XRF approaches usually compensate for a lack of knowledge about some or all of these parameters by conducting a calibration with respect to qualified calibration samples.[13,14] This sample-based approach may be based on a calibration performed in advance by the XRF device manufacturer to simplify usability, but may also include application-specific calibration schemes for more complex and demanding problems. For commercial XRF devices (commonly based on excitation by an X-ray tube), such sample-based calibration approaches are used exclusively. SR-based XRF approaches that rely on calibrated instrumentation and a knowledge of all contributing FPs do exist,[15] so-called reference-free XRF, but to date these have been limited to monochromatic excitation. Moreover, there are very few works that deal with the application of the calculation of the spectral distribution for polychromatic excitation by SR,[16,17] and none that discuss its general application to thin-film samples within a reference-free

Physikalisch-Technische Bundesanstalt, 10587 Berlin, Germany. E-mail: andre.waehlisch@ptb.de

† Electronic supplementary information (ESI) available. See DOI: https://doi.org/10.1039/d3ja00109a

‡ Present address: Helmut Fischer GmbH, Institut für Elektronik und Messtechnik, 12489 Berlin, Germany.

§ Present address: MPI für Chemische Energiekonversion, 45470 Mülheim an der Ruhr, Germany.

approach. In this work, we corroborate that such a reference-free quantification can be achieved reliably for polychromatic SR by utilizing the radiation from a well-characterized bending magnet, directly transferring the well-known principles of monochromatic excitation. Furthermore, we present a three-way comparison of (I) A reference-free XRF quantification based on monochromatized SR; (II) a reference-free XRF quantification based on polychromatic SR; and (III) an XRF quantification based on polychromatic radiation from an X-ray tube and utilizing calibration samples. It is shown that while all three approaches produce reliable quantification results for thin layers and stratified materials, they have distinct advantages and disadvantages. We will additionally consider how the general principles of the reference-free approach can be transferred to the laboratory using X-ray tube-based devices.

2 Experimental setups

2.1 Reference-free XRF based on monochromatic SR

Experiments based on monochromatized SR were conducted at the 7 T wavelength-shifter beamline[18] at *BESSY II*, an electron storage ring for SR. This beamline provides monochromatic X-ray radiation by means of a combination of a double-crystal and a double-multilayer monochromator. This combination results in a good energy resolution while maintaining high spectral purity. Here, we utilized an excitation photon energy of $E_0 = 13$ keV. A schematic view of the experimental setup is shown in Fig. 1. The beamline includes several common beam altering components aside from the monochromators. These components include several apertures at different positions to reduce stray light contributions, beam absorbers to improve the spectral purity, and an ionization chamber to monitor the photon flux of the incident radiation $\Phi_0(E_0)$ upstream of the experiment. Because of the general complexity of a beamline, and in particular of its optical components, it would not be straightforward to calculate the absolute value of $\Phi_0(E_0)$ based on the radiation emitted by the wavelength-shifter radiation source. But the related radiant power can be easily determined with high accuracy by means of a calibrated photodiode[19] located downstream of the sample position, provided that the radiation is sufficiently monochromatized to accommodate the photodiode's lack of energy discrimination capabilities. A calibrated

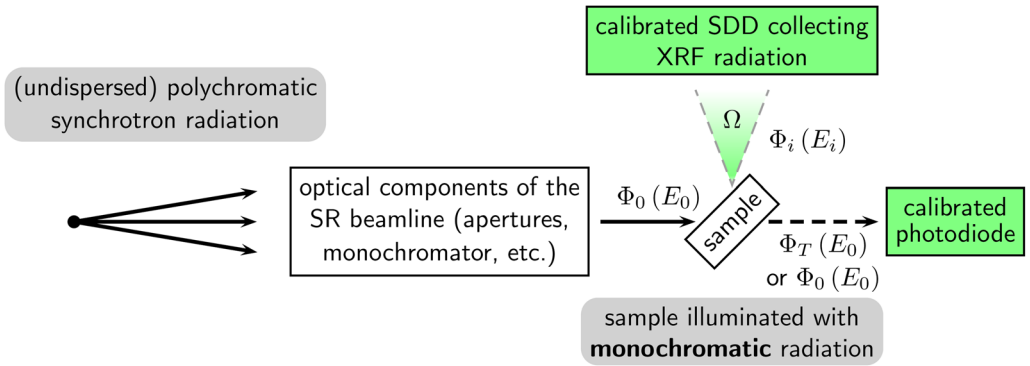

Fig. 1 Schematic drawing of the experimental setup used for reference-free SRXRF based on monochromatic radiation. The reference-free approach relies on the calibration of the colourized parts, namely the solid angle of detection, an SDD, and a photodiode.

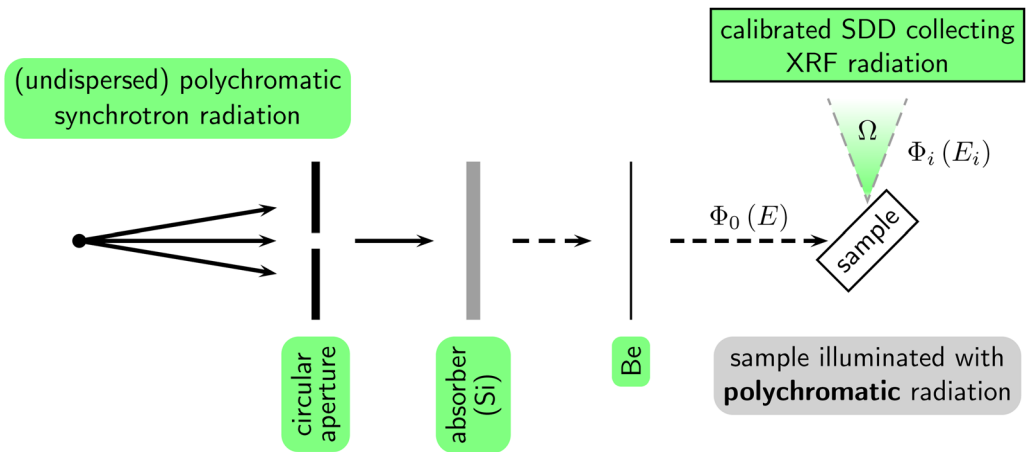

Fig. 2 Schematic drawing of the experimental setup used for reference-free SRXRF based on polychromatic radiation. The reference-free approach relies on the calibration of the colourized parts, namely the solid angle of detection, an SDD, and the components related to the excitation source.

silicon drift detector (SDD) is used for the detection of the characteristic lines of the elements contained within the sample investigated, *i.e.*, SR-based XRF (SRXRF). The detector is placed in the plane of the storage ring and at a right angle to the incident radiation. This arrangement strongly reduces undesirable contributions due to scattering from the sample because the SR is linearly polarized in the storage ring plane. The SDD was radiometrically calibrated[20,21] so its response behaviour and detection efficiency are well-known. These are prerequisites for the reference-free approach. The samples were aligned such that the angles of incidence and detection were 45°. The complete setup, including beamline, sample chamber, and SDD, is realized in ultra-high vacuum (UHV) to avoid attenuation of the X-ray radiation by air.

2.2 Reference-free XRF based on polychromatic SR

Reference-free XRF measurements based on polychromatic SR were conducted at the beamline for undispersed bending magnet radiation[22] in the PTB laboratory, which is also located at *BESSY II*. This beamline is primarily dedicated to the calibration of X-ray detectors, including SDDs.[23–26] A schematic view of the experimental setup is shown in Fig. 2. The beamline provides direct access to the radiation of a 1.3 T bending magnet and employs no optical elements except a single calibrated aperture and optional well-characterized beam absorbers.

The circular aperture is installed at a known distance from the radiation source point of the bending magnet (29 120(6) mm) and defines the solid angle of the radiation illuminating the samples. The area of the aperture was calibrated by means of an optical microscope (approximately 0.8 mm^2). Furthermore, the aperture was mounted on a linear stage enabling vertical alignment with regard to the plane of the electron orbit of the synchrotron radiation facility. A beam absorber can be introduced into the beam path—downstream from the aperture—to attenuate the high photon flux generated by the bending magnet. The non-attenuated photon flux is generally more than 10^{13} s^{-1} behind the aperture during the standard operation modus of *BESSY II* (ring current ≈ 300 mA). Indeed, avoiding detector dead times and even beam damage for this high photon flux would require impractical detector distances or impossibly thin samples. Instead, a beam absorber (a stack of three pure Si wafers) is employed that reduces the incident photon flux Φ_0 by several orders of magnitude over the complete spectral range. For the following calculations, this absorber is taken into account by means of Beer's attenuation law for the transmitted photon flux $\Phi_T(E) = \Phi_0(E)\exp[-\mu(E)\rho d(\sin\theta_{in})^{-1}]$, which incorporates the thickness of the absorber d, its mass attenuation coefficient $\mu(E)$, the density ρ of the material, and the angle of incidence θ_{in}. While d was determined experimentally with the use of a digital caliper (2.22(5) mm), μ and ρ are taken from the literature.[27] Given that the absorber significantly alters the spectral distribution of the incident radiation, it is crucial for the following quantifications that this absorber be of high chemical purity or, alternatively, that one has accurate knowledge of the composition of the absorber material. The purity of the wafers was verified by SRXRF (see the ESI†). The effect of unwanted excitation of the sample due to secondary radiation from the absorber—*i.e.*, scattered radiation and X-ray fluorescence radiation emitted by the absorber material itself—is minimized by utilizing a moderately large distance between the absorber and the sample (>1 m). Moreover, a thin beryllium foil (about 125 μm) separates the vacuum of the beamline from that of the experimental end-station—mainly for practical reasons—and has only minor impact on the relevant parts of the incident radiation here.

Samples were mounted in an UHV-compatible chamber similar to the one presented by Lubeck *et al.*[28,29] This chamber is equipped with a sample manipulator which enables precise translational and rotational alignment of the samples with regard to the incident radiation defined by the circular aperture. Identical to the experiments performed with monochromatized SR, a calibrated SDD was used to collect the emitted X-ray fluorescence radiation.

2.3 XRF based on polychromatic radiation from an X-ray tube

For ease of comparison with the most commonly used approach in the context of XRF, the following reference-free results are compared with a commercial bench-top instrument which is

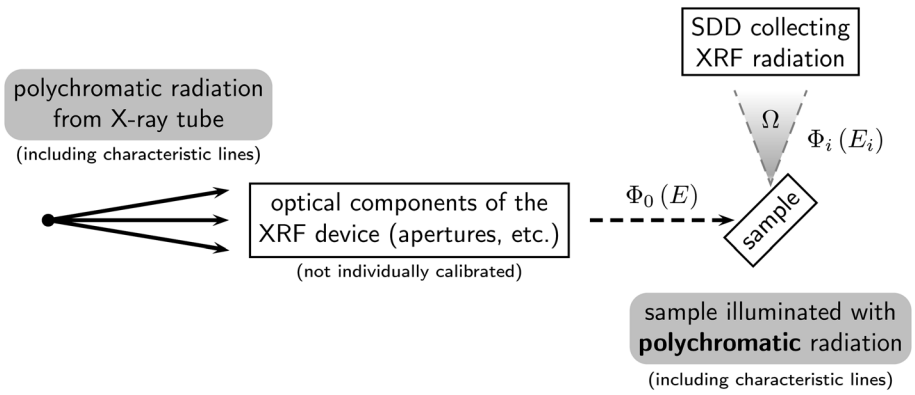

Fig. 3 Schematic drawing of the experimental setup used for XRF based on an X-ray tube. Optical components of the XRF device include an aperture and an absorber.

based on traditional X-ray tube excitation conditions and industry standard calibration schemes. These experiments were carried out on a *FISCHERSCOPE* XRF instrument. The simplified experimental setup is shown in Fig. 3. The X-ray radiation emitted by a tungsten anode is used to illuminate the samples, which are placed behind an absorber (500 μm aluminium) and an aperture. The tube voltage was set to 50 kV and the tube current was in the order of about 1 mA. The XRF radiation emitted by the samples was collected by an (uncalibrated) SDD. The average of 10 repeated measurements (30 s each) gave a relative standard deviation of less than 0.5 %.

The device manufacturer provided software that performed the quantification based on a sample-based calibration scheme that required minimal user intervention. As is very common with commercial XRF instruments, individual instrumental parameters are *not* calibrated. In contrast to the reference-free approach, they are only implicitly determined. Rather, quantitative results are derived by comparing the intensity of the detected X-ray fluorescence radiation with that of one or more well-known samples. The intensity data required for this form of calibration is usually predetermined by the manufacturer of the device, reducing the need for user intervention. An additional sample-based calibration can usually also be performed to address application-specific requirements or long-term stability issues, but was not used for the measurements presented.

3 Samples

The samples analysed for the present work were free-standing pure copper and titanium foils. The foils had a nominal thickness of 2 μm and 4 μm, respectively. In addition, an artificial bilayer was created by stacking the titanium foil on top of the copper foil. In this case, the copper X-ray fluorescence radiation may induce secondary titanium X-ray fluorescence radiation.[30] Differences in the lateral homogeneity of both foils were characterized by μXRF and are in the range of a few percent (see the ESI†).

4 Reference-free XRF with calculable excitation

The rate at which primary detectable X-ray fluorescence photons are emitted by a pure specimen of mass thickness ρd (g cm^{-2}) when illuminated by monochromatic radiation can be derived by the following equation.[31] This takes into account all relevant instrumental, experimental, and atomic fundamental parameters:

$$\underbrace{\Phi_i(E_i) = \Phi_0(E_0)\frac{\Omega}{4\pi}\varepsilon_i\frac{1}{\sin\theta_{\mathrm{in}}}}_{\text{instrumental and experimental parameters}}\underbrace{\frac{Q_{i,E_0}}{\mu_{\mathrm{tot},i}}\left[1-\exp\left(-\mu_{\mathrm{tot},i}\overbrace{\rho d}^{\text{objective of quantification}}\right)\right]}_{\text{fundamental parameters}}. \quad (1)$$

Here, Φ_i is the photon flux of the X-ray fluorescence radiation with photon energy E_i, Φ_0 is the photon flux of the monochromatic incident radiation with photon energy E_0, Ω is the solid angle of detection, ε_i is the energy-dependent detection efficiency of the detector, θ_{in} the angle of incidence, Q_{i,E_0} the X-ray fluorescence production coefficient of the X-ray fluorescence line i (cm^2 g^{-1}; this includes fluorescence yield, transition probability, and photoionization coefficient), $\mu_{\mathrm{tot},i} = \mu_{\mathrm{tot},i}(E_0, E_i) = \frac{\mu_{E_0}}{\sin\theta_{\mathrm{in}}} + \frac{\mu_{E_i}}{\sin\theta_{\mathrm{out}}}$ with the mass attenuation coefficient μ (cm^2 g^{-1}). Similarly, absorption and secondary fluorescence effects[30,32–36] have to be included for multi-elemental samples.

Conversely, the mass thickness ρd can be easily derived from eqn (1) if the X-ray fluorescence intensity Φ_i is determined experimentally and all other instrumental, experimental, and atomic fundamental parameters are known.[15] This is the basis of reference-free XRF analysis. The rate at which primary fluorescence photons Φ_i are emitted from a pure sample when excited by polychromatic radiation is given by the integration of eqn (1) over the relevant photon energy interval:[14]

$$\Phi_i(E_i) = \frac{\Omega\varepsilon_i}{4\pi\sin\theta_{\mathrm{in}}}\int_{E_{\mathrm{abs},i}}^{\infty}\Phi_0(E)\frac{Q_{i,E}}{\mu_{\mathrm{tot},i}}\left[1-\exp\left(-\mu_{\mathrm{tot},i}\rho d\right)\right]\mathrm{d}E. \quad (2)$$

Here, $E_{\mathrm{abs},i}$ is the energy of the absorption edge, *i.e.*, the minimum energy required for the corresponding ionization. To derive the parameters of interest for a multi-elemental sample, the elemental mass thicknesses ($\rho d = \sum_i \rho_i d_i$), a set of equations similar to eqn (2) is usually solved with a non-linear optimization algorithm. As can be seen from eqn (2), the photon flux $\Phi_0(E)$ at every relevant photon energy E needs to be known for this purpose. For monochromatic excitation, the incident photon flux can be easily determined using calibrated instrumentation.[15] The following paragraph below will describe how the excitation spectrum can be accurately calculated when using the polychromatic SR from a bending magnet. For other different polychromatic X-ray sources, theoretical descriptions are usually employed to estimate the excitation spectrum, as any specific measurement of this spectrum[37] is only valid for a single experimental setting and may be subject to stability issues. Nevertheless, there are several approaches for calculating the excitation spectra of laboratory-based X-ray tube instruments.[38–45] These approaches can be empirically verified or calibrated, and the stability of the instrument monitored, for example, by using well-characterized calibration samples. In principle, the utilization of a calculable excitation spectrum can be applied to any X-ray radiation source. While many commercial XRF devices are capable of applying approaches

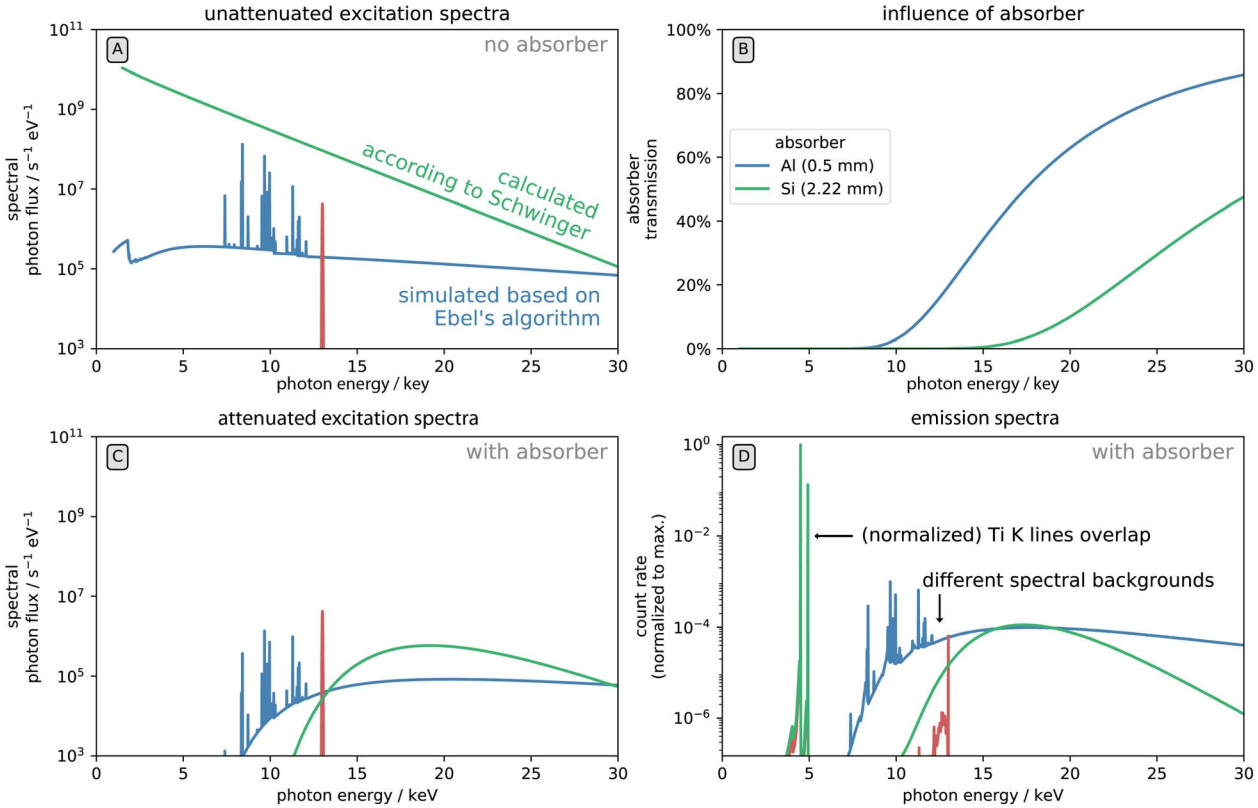

Fig. 4 Comparison of theoretical spectra for the comparison of the three X-ray excitation sources (X-ray tube, undispersed SR, monochromatized SR). (A) Theoretical excitation spectra of the three X-ray sources. (B) Theoretical influence of the respective absorber materials used during the measurements. The Si absorber is used for the measurement based on undispersed SR and the Al absorber for the X-ray tube measurements. (C) Theoretical excitation spectra from subfigure (A) after including the influence of the absorber materials. (D) Theoretical emission spectra of the sample. These spectra are based on the excitation spectra shown in subfigure (C) for a 4 μm thick titanium foil and are normalized to the titanium K_α line for better comparability. All of these spectra are based on typical experimental conditions as described in the text.

based on using fundamental parameters (sometimes called standardless or standard-free approaches) a completely reference-free approach is only feasible if also all instrumental and experimental parameters are determined. Despite the fact that examples for the calibration of individual instrumental parameters of commercial XRF instruments can be found in the literature (for example, for the solid angle of detection,[46] for the absolute excitation spectrum in terms of the spectral photon flux,[47] and for the spectral efficiency of the detector[20,23,48]), to the best of our knowledge, no reference-free approach has yet been demonstrated for X-ray tube instruments. In general, the reference-free approach is not inherently superior to a sample-based calibration approach, for example, with regard to the measurement uncertainties. In fact, relative measurements are usually associated with lower uncertainties than absolute measurements. The application-independent flexibility of the reference-free approach is, however, a major advantage when faced with changes in the experimental measurement setup or new material systems. Most crucially, since the reference-free approach relies on calibrated instrumentation, it is independent of details related to individual samples or types of sample systems.

The spectral flux of the SR emitted by a bending magnet can be calculated with low uncertainties, making the electron storage ring *BESSY II* a suitable primary source standard.[49] This calculation is based on Schwinger's theory[50] for the emission spectrum of an electron passing through a bending magnet with relativistic velocity.[51] Extracting a quantitative result from this theory requires knowledge of multiple storage ring parameters, *i.e.*, energy of the electrons, magnetic induction at the radiation source point, and electron beam current during the experiment. For *BESSY II*, these parameters are readily available based on the previous work of Thornagel *et al.*,[49] who established most of the experimental realization and equipment needed for determining the respective parameters. Furthermore, the effective solid angle of the incident radiation and its specific spatial location with respect to the sample needs to be known. This may be defined by the diameter of an aperture, the distance of this aperture from the source point, and the vertical offset of the aperture to the plane of electron orbit in the electron storage ring. Since the X-ray radiation emitted by a bending magnet has its maximum intensity in the electron–orbit plane, the offset is usually minimized in the experiment.

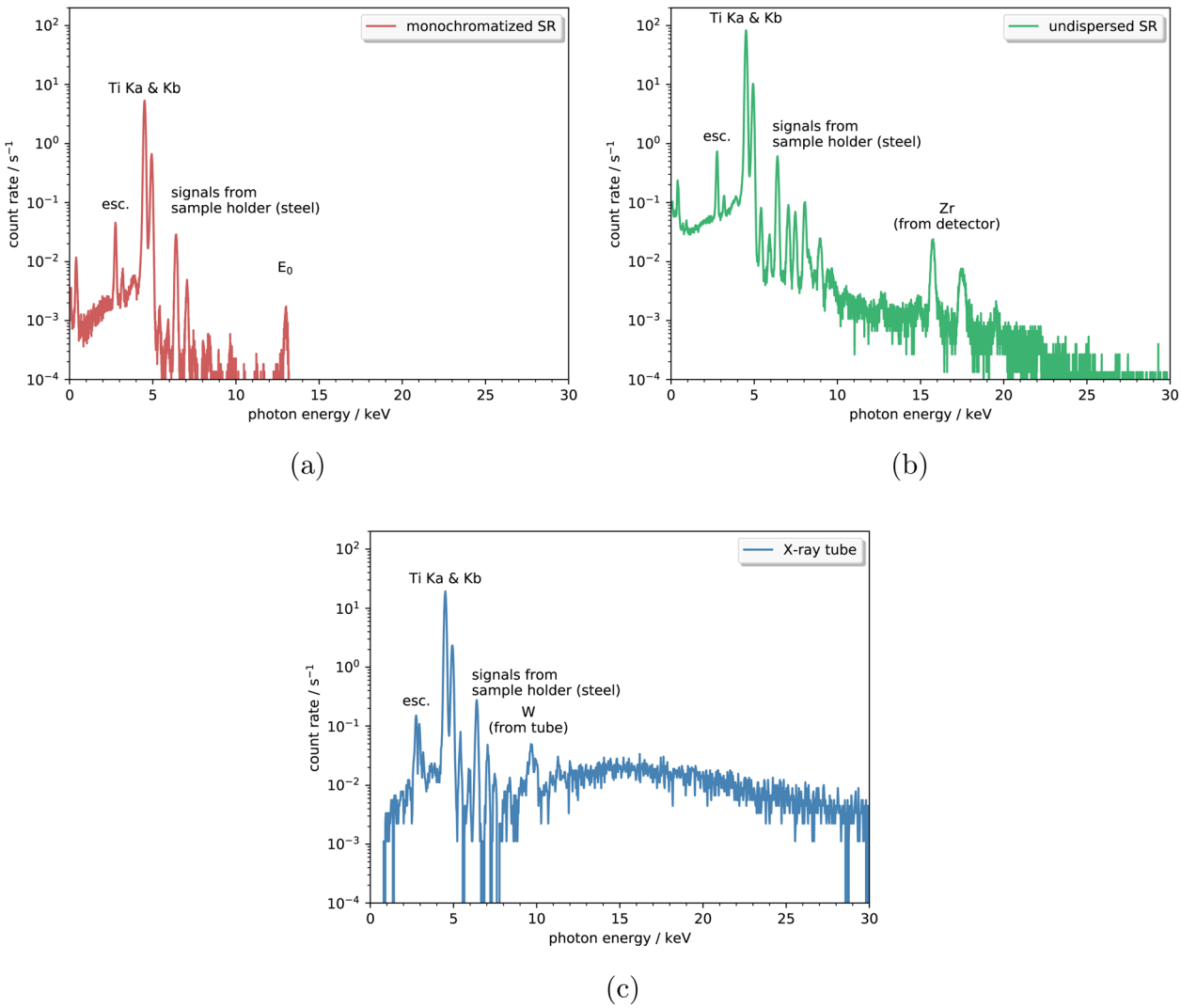

Fig. 5 Experimental spectra of 4 μm titanium sample. Negligible signal from the steel sample holder is visible as indicated in the figures (mainly Cr, Mn, Fe, Ni, Cu). The escape peak associated with the titanium K lines (*esc.*) and the elastic Rayleigh scattering peak (E_0) are also indicated.

5 Results

In order to demonstrate the general differences between the three X-ray excitation sources under consideration (X-ray tube, undispersed SR, monochromatized SR), their theoretical excitation spectra are compared in Fig. 4. The theoretical spectra of the X-ray tube (blue) were derived based on the free software package *XMI-MSIM*,[52] which implements the algorithm published by Ebel.[41,42] Parameters of the X-ray tube were set to values which may be encountered during standard operation of an XRF device equipped with a tungsten anode (tube current of 1 mA, tube voltage of 50 kV, and tube solid angle of 1 msr). While Fig. 4A illustrates the unattenuated spectra—without the influence of absorber materials as shown in Fig. 4B—the actual spectra which would be available on the sample are shown in Fig. 4C. It is evident that the excitation spectrum of the X-ray tube is very similar to a superposition of the spectrum of the undispersed (polychromatic) SR and the monochromatized SR. Namely, the spectrum of the X-ray tube has a polychromatic component (due to bremsstrahlung) and several monochromatic components, *i.e.*, the tungsten X-ray fluorescence lines.

Fig. 4D shows theoretical XRF spectra of a 4 μm thick titanium foil based on the three excitation spectra of Fig. 4C. These theoretical spectra are calculated by a Monte Carlo simulation based on *XMI-MSIM*. The software can simulate the photon paths emitted by an arbitrary excitation source. It then derives the interaction probabilities with a sample for photoionization,¶ Rayleigh scattering, and Compton scattering based on the FPs tabulated in the *xraylib* database.[27] Lastly, the software determines the number of photons reaching the detector. All three spectra shown in Fig. 4D contain the main quantitative information about the sample in the form of the titanium K

¶ It is worth noting that *XMI-MSIM* does not simulate bremsstrahlung generated by photoelectrons inside a specimen. This effect can contribute significantly to the total X-ray radiation emitted by a sample and, in that case, further increases the differences in spectral background for the three X-ray sources.

Table 1 Comparison of quantification results in terms of thicknesses. These determined thicknesses are derived by using the respective bulk density. Available standard uncertainty values are indicated in brackets. The software of the commercial XRF device based on X-ray tube excitation did not provide uncertainty values for its results. However, the number of significant digits was directly adopted as given by the software

Sample	Thickness/μm (due to monochr. SR)	Thickness/μm (due to undisp. SR)	Thickness/μm (due to X-ray tube)
Cu foil (individual)	2.1(2)	2.4(3)	2.12
Ti foil (individual)	3.7(3)	4.0(5)	3.66
Cu foil (in bilayer)	2.0(3)	2.4(5)	—
Ti foil (in bilayer)	3.6(3)	4.0(5)	—

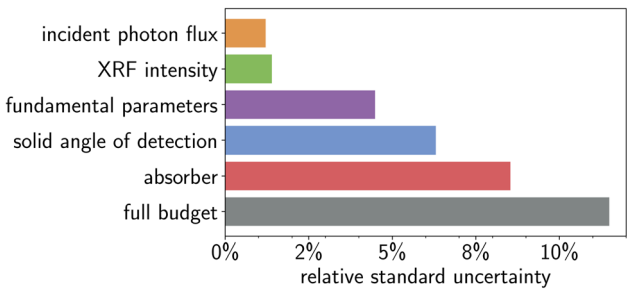

Fig. 6 Individual relative standard uncertainties and total relative standard uncertainty of the quantification results based on undispersed synchrotron radiation.

fluorescence lines, and they also contain information about the respective excitation source. The spectral distribution of each excitation source is affected by Rayleigh and Compton scattering in the sample, and these contributions would commonly be identified as spectral background to the titanium X-ray fluorescence signal. Indeed, the contributions of the spectral background differ substantially for the three different types of X-ray sources. Consequently, it is reasonable to expect different quantification capabilities for the three different X-ray sources, given that they have different detection limits on both an absolute and relative scale.

The actual experimental spectra of the 4 μm titanium foil are shown in Fig. 5 for the three different X-ray excitation sources. In principle, these experimental spectra correspond to the theoretical XRF spectra shown in Fig. 4 after being convolved with the detector response function and taking into account the energy-dependent detector efficiency (with the addition of contributions due to bremsstrahlung and stray light from the sample holder). As mentioned above, the three XRF spectra show a distinctly different spectral distribution of the background. This background is mainly due to scattering of the excitation radiation and bremsstrahlung created in the sample. Because the SR is linearly polarized, the contribution due to scattering can be greatly reduced by the chosen spatial placement of the detector.[9,53] Furthermore, the spectrum corresponding to the monochromatic SR excitation has the lowest spectral background because only a single monochromatic component contributes to the scattering process.

Table 1 shows the quantitative results of the titanium sample derived from the spectra shown in Fig. 5. Additionally, it lists the results of the copper and the stratified sample (spectra not shown here). The results for all three different excitation approaches agree well within the experimental uncertainties. The corresponding uncertainty budget for the quantification results based on the undispersed synchrotron radiation is shown in Fig. 6 (see the ESI† for more details). It should be noted that the uncertainty associated with the absorber provides the largest contribution. Consequently, it is crucial to determine the influence of the absorber's transmission over the relevant energy range. The uncertainty budget for the quantification with monochromatic SR mostly includes similar uncertainty components (solid angle of detection, XRF intensity, FPs) but does not rely on knowledge of an absorber and, therefore, has a lower total uncertainty. Details about the uncertainty related to the commercial XRF device are not available.

6 Conclusion

In summary, this work demonstrates that a reference-free XRF quantification based on polychromatic X-ray radiation can be reliably realized. The knowledge about the spectral distribution of the excitation source can be integrated into the FP-based approach—previously limited to monochromatic excitation—if good knowledge on the relevant FPs is available for a broad energy range. While there are major differences between different excitation sources with regard to their spectral intensity and background, and hence to their limits of detection and quantification reliability, the same general principles may be applied. Consequently, this approach can be readily transferred from the application at a synchrotron radiation facility to more common sources of X-ray radiation, such as XRF instruments equipped with an X-ray tube. Provided that the spectral distribution of the polychromatic X-ray radiation source can be determined accurately on an absolute scale (downstream from any potential beam altering absorber material), the XRF quantification can directly be applied even to new materials without the effort otherwise required of qualifying new calibration samples.

Conflicts of interest

There are no conflicts to declare.

Acknowledgements

This work was supported by the European Partnership on Metrology, co-financed by the European Union's Horizon

Europe Research and Innovation Programme and by the Participating States through grant agreement 21GRD01 (OpMetBat).

References

1 C. Vanhoof, J. R. Bacon, U. E. A. Fittschen and L. Vincze, 2020 atomic spectrometry update – a review of advances in X-ray fluorescence spectrometry and its special applications, *J. Anal. At. Spectrom.*, 2020, **35**(9), 1704–1719.
2 S. Carter, R. Clough, A. Fisher, B. Gibson and B. Russell, Atomic spectrometry update: review of advances in the analysis of metals, chemicals and materials, *J. Anal. At. Spectrom.*, 2022, **37**(11), 2207–2281.
3 B. P. von der Heyden, Shedding light on ore deposits: A review of synchrotron X-ray radiation use in ore geology research, *Ore Geol. Rev.*, 2020, **117**, 103328.
4 M. Cotte, A. Genty-Vincent, K. Janssens and J. Susini, Applications of synchrotron X-ray nano-probes in the field of cultural heritage, *C. R. Phys.*, 2018, **19**(7), 575–588.
5 W. Giurlani, E. Berretti, M. Innocenti and A. Lavacchi, Measuring the Thickness of Metal Coatings: A Review of the Methods, *Coatings*, 2020, **10**(12), 1211.
6 P. Hönicke, Y. Kayser, K. V. Nikolaev, *et al.*, Simultaneous Dimensional and Analytical Characterization of Ordered Nanostructures, *Small*, 2022, **18**(6), 2105776.
7 A. Revenko, A. Tsvetyansky and A. Eritenko, X-ray fluorescence analysis of solid-state films, layers, and coatings, *Radiat. Phys. Chem.*, 2022, **197**, 110157.
8 R. Sitko, Quantitative X-ray fluorescence analysis of samples of less than 'infinite thickness': Difficulties and possibilities, *Spectrochim. Acta, Part B*, 2009, **64**(11), 1161–1172.
9 B. M. Gordon, Sensitivity calculations for multielemental trace analysis by synchrotron radiation induced X-ray fluorescence, *Nucl. Instrum. Methods Phys. Res.*, 1982, **204**(1), 223–229.
10 A. Iida, K. Sakurai, T. Matsushita and Y. Gohshi, Energy dispersive X-ray fluorescence analysis with synchrotron radiation, *Nucl. Instrum. Methods Phys. Res., Sect. A*, 1985, **228**(2), 556–563.
11 P. Ketelsen, A. Knöchel and W. Petersen, Synchrotron radiation excited X-ray fluorescence analysis using a graphite monochromator, *Fresenius' Z. Anal. Chem.*, 1986, **323**(8), 807–810.
12 C. Streli, P. Wobrauschek, W. Ladisich, *et al.*, Total reflection X-ray fluorescence analysis of light elements using synchrotron radiation, *Nucl. Instrum. Methods Phys. Res., Sect. A*, 1994, **345**(2), 399–403.
13 T. Wolff, W. Malzer, I. Mantouvalou, O. Hahn and B. Kanngießer, A new fundamental parameter based calibration procedure for micro X-ray fluorescence spectrometers, *Spectrochim. Acta, Part B*, 2011, **66**(2), 170–178.
14 M. Mantler, Quantitative Analysis, in *Handbook of Practical X-Ray Fluorescence Analysis*, ed. B. Beckhoff, B. Kanngießer, N. Langhoff, R. Wedell, and H. Wolff, Springer, 2006.
15 B. Beckhoff, Reference-free X-ray spectrometry based on metrology using synchrotron radiation, *J. Anal. At. Spectrom.*, 2008, **23**, 845–853.
16 A. Knöchel, W. Petersen and G. Tolkiehn, X-ray fluorescence spectrometry with synchrotron radiation, *Anal. Chim. Acta*, 1985, **173**, 105–116.
17 F. Pantenburg, T. Beier, F. Hennrich and H. Mommsen, The fundamental parameter method applied to X-ray fluorescence analysis with synchrotron radiation, *Nucl. Instrum. Methods Phys. Res., Sect. B*, 1992, **68**(1), 125–132.
18 H. Riesemeier, K. Ecker, W. Görner, B. R. Müller, M. Radtke and M. Krumrey, Layout and first XRF applications of the BAMline at BESSY II, *X-Ray Spectrom.*, 2005, **34**(2), 160–163.
19 A. Gottwald, U. Kroth, M. Krumrey, M. Richter, F. Scholze and G. Ulm, The PTB high-accuracy spectral responsivity scale in the VUV and x-ray range, *Metrologia*, 2006, **43**(2), S125.
20 F. Scholze and M. Procop, Detection efficiency of energy-dispersive detectors with low-energy windows, *X-Ray Spectrom.*, 2005, **34**, 473–476.
21 F. Scholze and M. Procop, Modelling the response function of energy dispersive X-ray spectrometers with silicon detectors, *X-Ray Spectrom.*, 2009, **38**, 312–321.
22 G. Ulm, B. Beckhoff, R. Klein, M. Krumrey, H. Rabus, and R. Thornagel, PTB radiometry laboratory at the BESSY II electron storage ring, in *X-Ray Optics, Instruments, and Missions*, International Society for Optics and Photonics. SPIE, 1998, vol. 3444, pp. 610–621.
23 B. Beckhoff, R. Klein, M. Krumrey, F. Scholze, R. Thornagel and G. Ulm, X-ray detector calibration in the PTB radiometry laboratory at the electron storage ring BESSY II, *Nucl. Instrum. Methods Phys. Res., Sect. A*, 2000, **444**, 480–483.
24 M. Krumrey and G. Ulm, High-accuracy detector calibration at the PTB four-crystal monochromator beamline, in *Proceedings of the 7th Int. Conf. on Synchrotron Radiation Instrumentation*, 2001, vol. 467–468, pp. 1175–1178.
25 M. Krumrey, M. Gerlach, F. Scholze and G. Ulm, Calibration and characterization of semiconductor X-ray detectors with synchrotron radiation, *Nucl. Instrum. Methods Phys. Res., Sect. A*, 2006, **568**(1), 364–368.
26 B. Beckhoff, A. Gottwald, R. Klein, *et al.*, A quarter-century of metrology using synchrotron radiation by PTB in Berlin, *Phys. Status Solidi B*, 2009, **246**, 1415–1434.
27 T. Schoonjans, A. Brunetti, B. Golosio, *et al.*, The xraylib library for X-ray–matter interactions. Recent developments, *Spectrochim. Acta, Part B*, 2011, **66**(11), 776–784.
28 J. Lubeck, B. Beckhoff, R. Fliegauf, *et al.*, A novel instrument for quantitative nanoanalytics involving complementary X-ray methodologies, *Rev. Sci. Instrum.*, 2013, **84**, 045106.
29 J. Lubeck, M. Bogovac, B. Boyer, *et al.*, A New Generation of X-ray Spectrometry UHV Instruments at the SR Facilities BESSY II, ELETTRA and SOLEIL, *AIP Conf. Proc.*, 2016, **1741**, 030011.
30 A. Wählisch, C. Streeck, P. Hönicke and B. Beckhoff, Validation of secondary fluorescence excitation in quantitative X-ray fluorescence analysis of thin alloy films, *J. Anal. At. Spectrom.*, 2020, **35**, 1664–1670.

31 J. Sherman, The theoretical derivation of fluorescent X-ray intensities from mixtures, *Spectrochim. Acta*, 1955, **7**, 283–306.
32 M. Mantler, LAMA III – A Computer Program For Quantitative XRFA of Bulk Specimens and Thin Film Layers, *Adv. X-Ray Anal.*, 1984, **27**, 433–440.
33 M. Mantler, X-ray fluorescence analysis of multiple-layer films, *Anal. Chim. Acta*, 1986, **188**, 25–35.
34 T. Shiraiwa and N. Fujino, Theoretical Calculation of Fluorescent X-Ray Intensities in Fluorescent X-Ray Spectrochemical Analysis, *Jpn. J. Appl. Phys.*, 1966, **5**(10), 886.
35 D. K. G. de Boer, Calculation of x-ray fluorescence intensities from bulk and multilayer samples, *X-Ray Spectrom.*, 1990, **19**(3), 145–154.
36 D. K. G. de Boer, J. J. M. Borstrok, A. J. G. Leenaers, H. A. Van Sprang and P. N. Brouwer, How accurate is the fundamental parameter approach? XRF analysis of bulk and multilayer samples, *X-Ray Spectrom.*, 1993, **22**(1), 33–38.
37 H. Aiginger, M. Benedikt and R. Görgl, Energy Dispersive Measurement of X-Ray Tube Spectra, *Adv. X-Ray Anal.*, 1995, **39**, 137–147.
38 P. A. Pella, L. Feng and J. A. Small, An analytical algorithm for calculation of spectral distributions of x-ray tubes for quantitative x-ray fluorescence analysis, *X-Ray Spectrom.*, 1985, **14**(3), 125–135.
39 P. A. Pella, L. Feng and J. A. Small, Addition of M- and L-series lines to NIST algorithm for calculation of x-ray tube output spectral distributions, *X-Ray Spectrom.*, 1991, **20**(3), 109–110.
40 A. L. Finkelshtein and T. O. Pavlova, Calculation of x-ray tube spectral distributions, *X-Ray Spectrom.*, 1999, **28**(1), 27–32.
41 H. Ebel, X-ray tube spectra, *X-Ray Spectrom.*, 1999, **28**(4), 255–266.
42 H. Ebel, Lι, Lα1,2, Lη, Lβ1,2,3,4,5,6 and Lγ1,2,3 spectra of x-ray tubes, *X-Ray Spectrom.*, 2003, **32**(1), 46–51.
43 G. G. Poludniowski and P. M. Evans, Calculation of x-ray spectra emerging from an x-ray tube. Part I. Electron penetration characteristics in X-ray targets, *Med. Phys.*, 2007, **34**(6), 2164–2174.
44 G. G. Poludniowski, Calculation of x-ray spectra emerging from an x-ray tube. Part II. X-ray production and filtration in x-ray targets, *Med. Phys.*, 2007, **34**(6), 2175–2186.
45 V. Rackwitz, U. Panne and V.-D. Hodoroaba, Calculation of X-ray tube spectra by means of photon generation yields and a modified Kramers background for side-window X-ray tubes, *X-Ray Spectrom.*, 2012, **41**(4), 264–272.
46 P. Hönicke, U. Waldschläger, T. Wiesner, M. Krämer and B. Beckhoff, Towards a calibration of laboratory setups for grazing incidence and total-reflection X-ray fluorescence analysis, *Spectrochim. Acta, Part B*, 2020, **174**, 106009.
47 V. Rackwitz, A. Warrikhoff and V.-D. Hodoroaba, Accurate determination of small spot X-ray tube spectra by means of direct measurement in a calibrated instrumental setup, *J. Anal. At. Spectrom.*, 2014, **29**(3), 458–463.
48 M. Alvisi, M. Blome, M. Griepentrog, *et al.*, The Determination of the Efficiency of Energy Dispersive X-Ray Spectrometers by a New Reference Material, *Microsc. Microanal.*, 2006, **12**(5), 406–415.
49 R. Thornagel, R. Klein and G. Ulm, The electron storage ring BESSY II as a primary source standard from the visible to the X-ray, *Metrologia*, 2001, **38**(5), 385–389.
50 J. Schwinger, On the Classical Radiation of Accelerated Electrons, *Phys. Rev.*, 1949, **75**(12), 1912–1925.
51 E. L. Shirley, M. Furst and U. Arp, Invited Article: Refined analysis of synchrotron radiation for NIST's SURF III facility, *Rev. Sci. Instrum.*, 2018, **89**(4), 041301.
52 T. Schoonjans, L. Vincze, V. A. Solé, *et al.*, A general Monte Carlo simulation of energy dispersive X-ray fluorescence spectrometers – Part 5: Polarized radiation, stratified samples, cascade effects, M-lines, *Spectrochim. Acta, Part B*, 2012, **70**, 10–23.
53 K. Sakurai, A. Iida and Y. Gohshi, Analysis of Signal to Background Ratio in Synchrotron Radiation X-Ray Fluorescence, *Anal. Sci.*, 1988, **4**(1), 3–7.